THE FIRE-INDUCED CEILING-JET REVISITED

Ronald L. Alpert
Alpert Fire Protection Science
rlalpert@alum.mit.edu

ABSTRACT: Data on near-maximum gas velocity and excess temperature in the ceiling jet induced by large-scale fires that were used to obtain well-known ceiling-jet formulas published in 1972 have been re-examined in light of knowledge on the virtual plume origin and the convective component of the fire heat release rate. The new data correlations developed from this re-examination are compared with the original correlations that were based on actual ceiling height above the top fuel surface and actual fire heat release rate, instead of being based on ceiling height above the virtual origin and on the convective heat release rate. A full description of these data is provided as well as a description of the methods used to revise the correlation. This ceiling-jet analysis, useful for the prediction of detection and activation times, is followed by a discussion of how the calculation of the interaction of fire-induced flows with droplet sprays is needed to predict droplet penetration to burning fuel surfaces as well as the total number of automatic spray devices activated during a fire. Finally, there is a brief discussion of how an intermediate-scale configuration of combustible surfaces can be used to investigate the flammability of materials and minimum required agent flux to control fire spread.

INTRODUCTION

The radially-outward gas motion produced by impingement of a fire plume on a flat, horizontal, unobstructed ceiling is often referred to as the fire-induced ceiling jet. Knowledge of this relatively fast moving, high temperature, smoke-laden under-ceiling gas flow above the quiescent ambient air is essential for predicting the activation time of ceiling mounted devices, such as fire detectors and fire sprinklers, as well as the final extent of devices activated after successful fire suppression. The proper activation of sprinkler protection, which includes an area of activated devices less than that which would challenge the supply capabilities of suppression agent, is very important to insurers of highly protected commercial/industrial facilities.

The author was employed by an engineering and research organization, Factory Mutual Research Corporation (FMRC), owned by a consortium of this type of insurers beginning in 1969. The need for better engineering methods for predicting such sprinkler activation behavior led to the establishment of a program of fundamental research on fire-induced flows at FMRC, including a project on predicting the characteristics of a ceiling jet.

This paper will describe some of the results of that ceiling jet project and how a portion of the original data can be re-analyzed to obtain improved flow correlations. Then, another project will be discussed that involved some of the first calculations of the flow field resulting from a fire plume directly below an activated sprinkler spray. That project demonstrated the practicality of calculating the amount of suppression agent arriving at the seat of a fire as well as the cooling effect of agent on the ceiling flow. Finally, an interesting test configuration will be described that allows the amount of delivered agent necessary to suppress a fire on a given material to be determined.

CEILING JET CORRELATIONS

Figure 1 is a schematic illustrating the result of the impingement of the buoyant, hot gas from a fire (the fire plume) on a ceiling. This geometry is obviously an idealization of what happens when there is a fire in a building at floor level and ignores obstructions by wall and ceiling beams. Also shown in the figure is a control volume used to develop an integral theory for predicting ceiling jet behavior, including changes in ceiling jet gas velocity, V, excess (value above ambient) temperature, $T-T_\infty$, and the distance below the ceiling where these quantities approach the ambient values, h (i.e., ceiling jet thickness). The development of this semi-analytical theory[1] for the V, $T-T_\infty$ and h quantities (see Figure 1) in the early 1970's seemed to spark an interest in making measurements of ceiling jet properties both in full-scale fires and in small-scale, laboratory simulations. During the development of the ceiling-jet theory, the author was urged to correlate data then becoming available from full-scale fire tests, using parameters suggested by the theoretical model. The final result of this correlation effort, without any detailed justification and description of the underlying experiments, was presented at a meeting of the National Fire Protection Association and then published[2] in 1972.

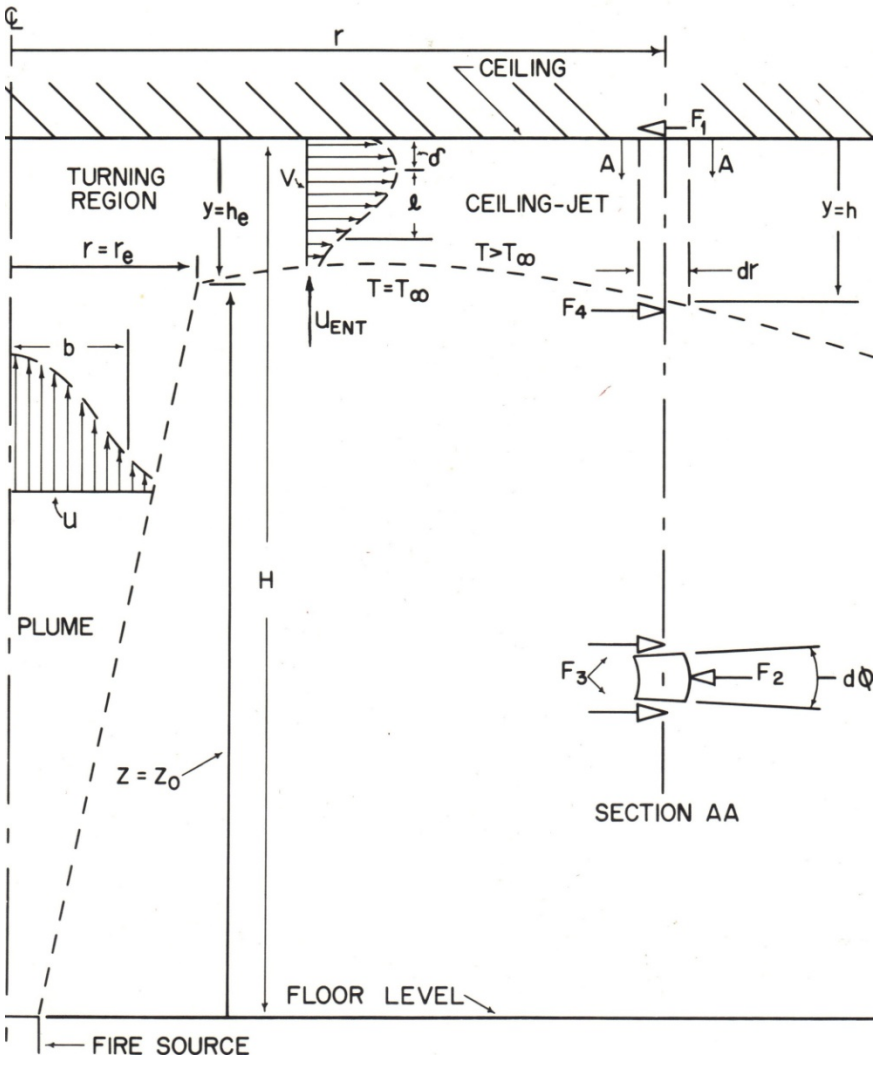

Figure 1 Schematic of Ceiling Jet Flow

Although the original formulas (see Equations 1 and 2) were presented without any experimental evidence, these relations seemed to be accepted as fact by many fire protection practitioners and even some researchers. One reason for this acceptance was an internal FMRC technical report[3] that had already been widely distributed to fire researchers in the USA and internationally in 1971. This report described the ceiling jet model, a few data points from a full-scale fire test and ample data from small-scale (yet mostly turbulent) laboratory experiments. Subsequent to this FMRC report, the author examined available data from a variety of full-scale fire tests, with the resultant correlations of these data, inspired by the ceiling jet model, shown in Figure 2 and Figure *3* for excess gas temperature and velocity, respectively.

Obviously, most of the fire sources used to obtain the correlations in Figure 2 and Figure ***3*** were not compatible with the assumptions of a point source of buoyancy at floor level, previously made to obtain the ceiling jet model. However, the data correlations were only being developed empirically and then a qualitative curve fit process (microcomputers were not yet available) was applied to arrive at Equations 1 and 2 that appeared in the 1972 publication[2].

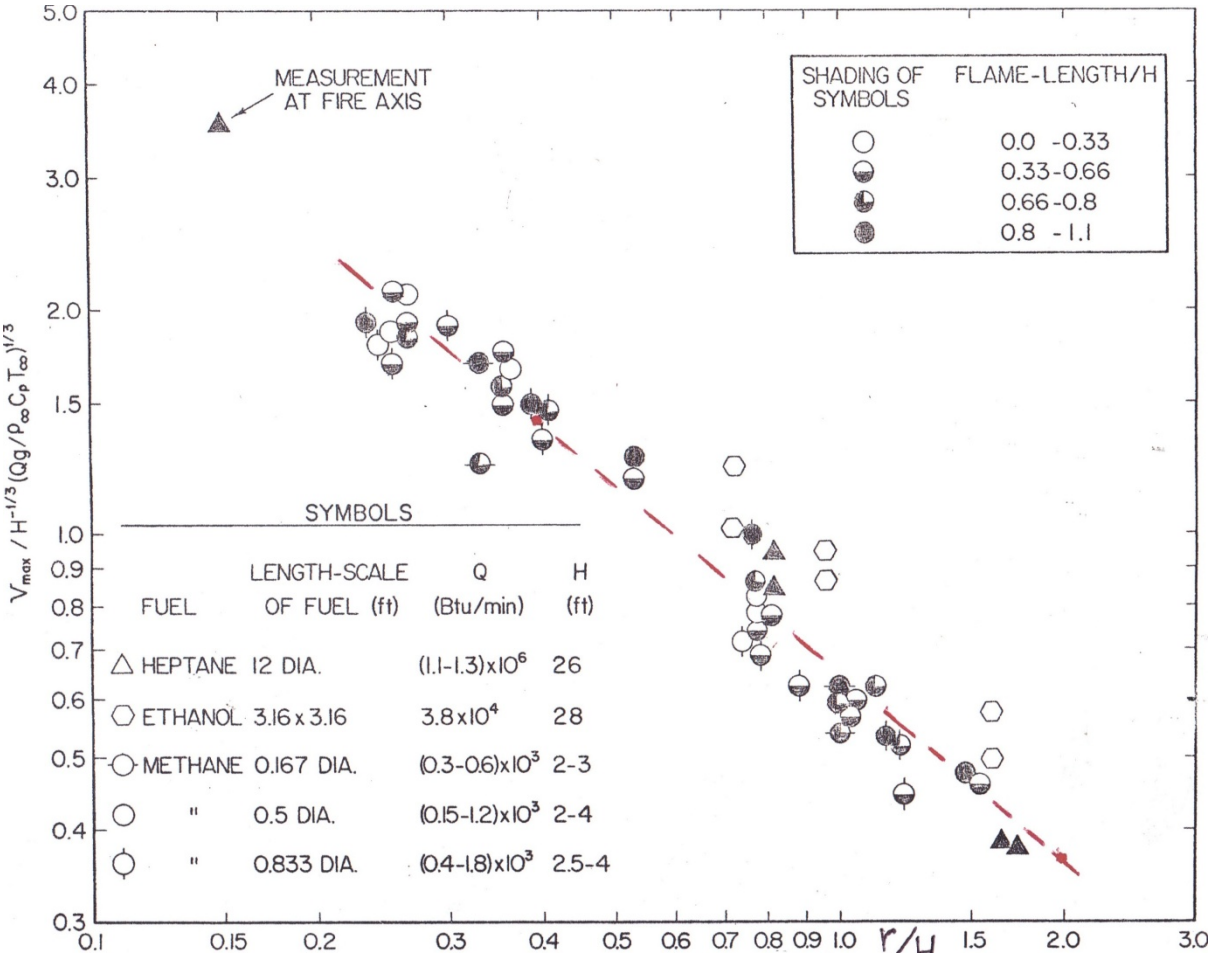

Figure 2 Nondimensional ceiling jet radial velocity vs. radial distance from the plume axis nondimensionalized by the ceiling height above the top fuel surface; this correlation is the basis for published formula[2], shown by the dashed line.

For these correlations, gas temperatures and velocities were measured by thermocouples and hot-wire anemometers, respectively, at several radial locations and at a few distances below the ceiling to be able to estimate maximum values. Most such measurements were finally made at about 150 mm or less below the ceiling. The heat release rate used in the ordinates was the product of measured mass loss rate from a load platform (or heptane flow rate in the case of the nozzle array) and an estimate of the actual value for heat of combustion during a typical fire, what is often now called the "chemical heat of combustion." Handbook values for this quantity based on standard laboratory calorimeter measurements were not available at that time. Note that the length scale used for the correlation was the ceiling height above the top surface of the fuel, which for the heptane sprays, was the height above the plane of the spray nozzles. Measurements were made in a very large test building in order to minimize the effects of ambient drafts and the accumulation of combustion products in a descending smoke layer.

In SI units (kW, m, ^{o}C, s), the formulas derived from the correlations in *Figure **2*** and*Figure **3*** and published in the 1972 article[2] are:

$$V = 0.197 \frac{\left(\frac{\dot{Q}}{H}\right)^{1/3}}{\left(\frac{r}{H}\right)^{5/6}} \quad r/H > 0.15 \tag{1}$$

$$T - T_{\infty} = 5.38 \frac{\frac{\dot{Q}^{2/3}}{H^{5/3}}}{\left(\frac{r}{H}\right)^{2/3}} \quad r/H > 0.18 \tag{2}$$

It is of interest to do a more objective analysis of the original ceiling jet velocity and temperature data, e.g., a regression fit instead of a qualitative one. Unfortunately, much of the original information used to calculate the data shown in Figure 2 and Figure *3* is not available to the author except for that associated with the five fuel types in Table 1. These include a well-defined liquid pool in a square metal pan (ethanol), three solid fuel arrays (piles of cardboard boxes or pallets) and a group of six, inward-facing spray nozzles positioned on a 3.66 m diameter pipe circle (heptane sprays).

The previously estimated values for chemical heat of combustion used for the five selected fuels are given in Table 1, along with the better-defined net heat of complete combustion[4] for these fuels. Note that for heptane, the original correlation simply used the net heat of complete combustion rather than a reduced value to compute actual heat release rates. This presumably was done based on the assumption that combustion efficiency in a liquid spray should be very high.

The fire source characteristics associated with each of the five fuel types are listed in Table 2, where the last two columns in the table are simply the product of the fifth column (fuel flow) and the corresponding heat of combustion columns in Table 1. To compare the size of the

various fires, an effective diameter is obtained from the equivalent area of a circular source, the heptane fire already being circular. Velocity and temperature correlations of the same type as in Figure 2 and Figure *3* are then computed from the available data and shown in Figure 4 through *Figure 7*.

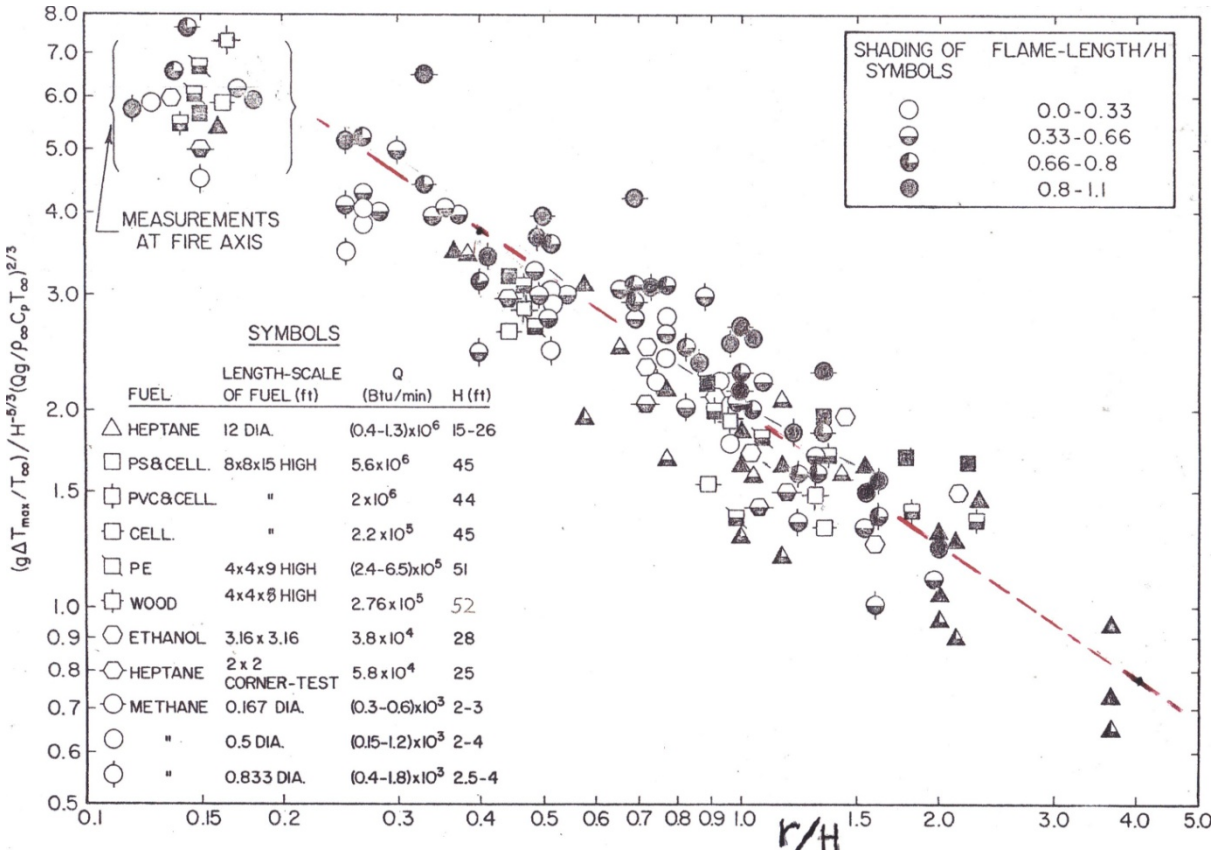

Figure 3 Nondimensional excess gas temperature vs. radial distance from the plume axis nondimensionalized by the ceiling height above the fuel surface; basis for published formula[2], shown by the dashed line. *Note that "PVC&Cell" stands for PVC & cellulose, an error that should have been "PE&Cell", for polyethylene & cellulose; similarly "PS&Cell" is polystyrene & cellulose.*

The ceiling jet velocity function in the ordinate of Figure 4 and Figure *5* is the dimensional quantity:

$$\frac{V_{\max}(H)^{1/3}}{\dot{Q}_{chem}^{1/3}} \quad \frac{m^{4/3}}{s \times kW^{1/3}}$$

And the ceiling jet excess temperature function in the ordinate of *Figure 6* and *Figure 7* is:

$$\frac{(T_{\max} - T_\infty)(H)^{5/3}}{\dot{Q}_{chem}^{2/3}} \quad \frac{K \times m^{5/3}}{kW^{2/3}}$$

In addition to the correlation of the original maximum velocity and temperature data, the figures contain power regression fits just to the data corresponding to ethanol (ethyl alcohol) fires, since these are the best defined fires sources. Note that in *Figure 6*, the excess temperature data corresponding to heptane spray fires have different symbols to differentiate the different fuel flow rates shown in Table 2 and, hence, flame lengths.

Fuel Type	*Net Heat of Complete Combustion*[4] *[kJ/g]*	*Chemical Heat of Combustion Used for Original Formula [kJ/g]*
Ethanol Pool	27.70	22.38
Wood Four-way Pallet Stack	16.4	13.96
Polyethylene Bottles in Compartmented Cardboard Boxes*	28.1	24.66
Polystyrene Jars in Compartmented Cardboard Boxes**	33.7	31.63
Heptane Sprays	44.6	44.6

*Table 1 Complete and Chemical (Actual) Heats of Combustion for the Selected Fuels, Using Values from the Original Correlation;*50.7% PE, 49.3% cardboard, ignoring pallets; **74.7% PS, 25.3% cardboard, ignoring pallets.*

Fuel Type	*Height of Burning Fuel [m]*	*Effective Diameter of Fuel [m]*	*Ceiling Height above Top of Fuel [m]*	*Fuel Flow or Mass Loss Rate [g/s]*	*Total HRR [kW]*	*Chemical HRR [kW]*
Ethanol Pool	0.00	1.09	8.61	24.18	669.8	541.15
Wood Four-way Pallet Stack	2.44	1.38	15.54	318.0	5,215	4,439
PE Bottles in Cardboard Boxes	4.57	2.77	13.41	1,390.5	39,034	34,290
PS Jars in Cardboard Boxes	4.11	2.94	13.87	3,113	104,752	98,464
Heptane Spray A	0.00	3.66	7.92	173.6	7,744	7,744
Heptane Spray B	0.00	3.66	7.92	303.8	13,551	13,551
Heptane Spray C	0.00	3.66	7.92	434.1	19,359	19,359
Heptane Spray D	0.00	3.66	7.92	520.9	23,231	23,231
Heptane Spray E	0.00	3.66	4.572	173.6	7,744	7,744
Heptane Spray F	0.00	3.66	4.572	303.8	13,551	13,551
Heptane Spray G	0.00	3.66	4.572	434.1	19,359	19,359

Table 2 Fire Source Conditions for the Selected Fuels from the Original Correlation

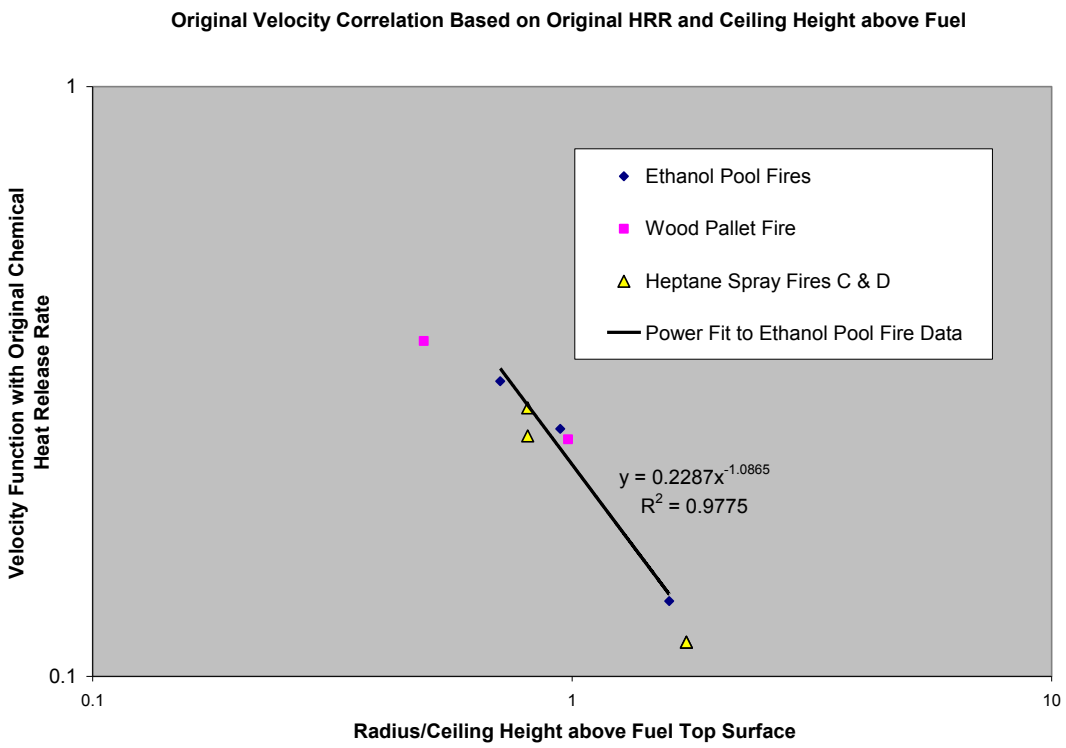

Figure 4 Re-analysis of Velocity Data for Selected Fuels from the Original Ceiling Jet Velocity Correlation

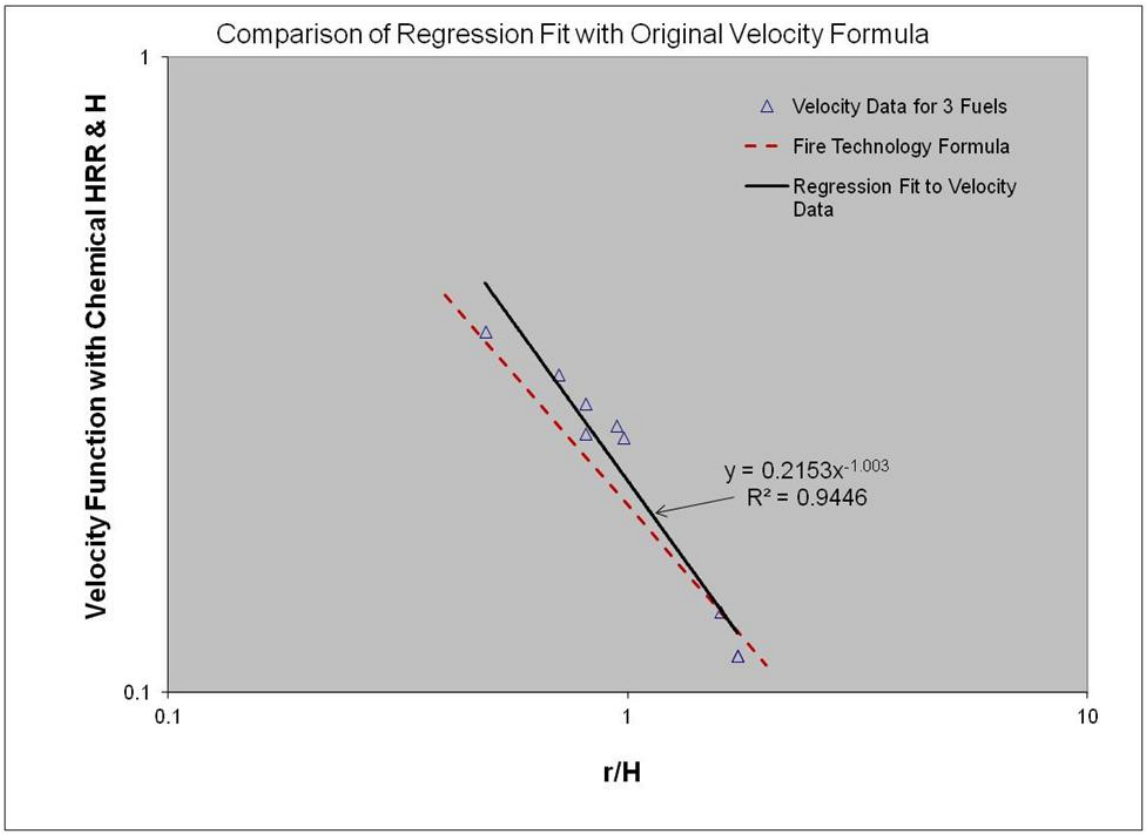

Figure 5 Comparison of Original Formula for Maximum Ceiling Jet Velocity with Regression Fit (solid line) to Data from Figure 4

The lowest ratio of flame height to ceiling height should correspond to heptane sprays A and B and the highest ratio to sprays F and G. Thus, data corresponding to the former set of sprays should perhaps be better correlated with the low flame ethanol pool fire data than data corresponding to the latter set of relatively high flames. Unfortunately, this does not seem to be the case, as data corresponding to heptane spray A are as well correlated with the ethanol data as those corresponding to spray G. However, data corresponding to heptane spray F are indeed far from the ethanol correlation fit.

When all of the fire sources from Table 1 are considered together, the power regression fit becomes as follows:

$$V = 0.215 \frac{\left(\frac{\dot{Q}_{chem}}{H}\right)^{1/3}}{\left(\frac{r}{H}\right)^{1.003}} \qquad R^2 = 0.945 \quad \text{(dashed line in } \textit{Figure 5}\text{)} \qquad (3)$$

$$T - T_\infty = 5.289 \frac{\frac{\dot{Q}_{chem}^{2/3}}{H^{5/3}}}{\left(\frac{r}{H}\right)^{0.611}} \qquad R^2 = 0.856 \quad \text{(dashed line in } \textit{Figure 7}\text{)} \qquad (4)$$

where Equations 3 and 4 now replace Equations 1 and 2 (from the 1972 paper[2]) as presumably more accurate versions, with the quantifiable regression coefficients (R^2 values) shown. It can be seen that, except for the power of r/H in the gas velocity correlation, the new regression fit is nearly identical to the original. The original power of r/H may have been selected with some degree of arbitrariness to obtain the rational number, 5/6.

Since the early 1970's, there has been a tremendous amount of progress made in understanding fire-induced flows, especially the plume generated by both simple pool fires as well as by much more complex fire sources. This work has been summarized by Heskestad[5], who has shown that the convective component of fire heat release rate, $\dot{Q}_{conv}$, governs the value of excess temperatures and velocities in the fire plume, rather than actual or chemical heat release rate.

In addition, a relationship has been developed[5] for the location of a virtual point source for fire plumes generated by simple, large area fuel surfaces, or complex fuel arrays in which there may be in-depth combustion. This virtual source relationship is valid as long as the origin for height measurement is at the lowest elevation where there is continuous flaming, rather than arbitrarily at the bottom or top surface of the fuel array. The virtual source concept allows previously established plume relations, such as those used in the original ceiling jet model, to still be valid as long as the point source location for all heat released is specified as in Equation 5.

$$z_v = 0.083 \dot{Q}_{chem}^{2/5} - 1.02 D_{eff} \qquad (5)$$

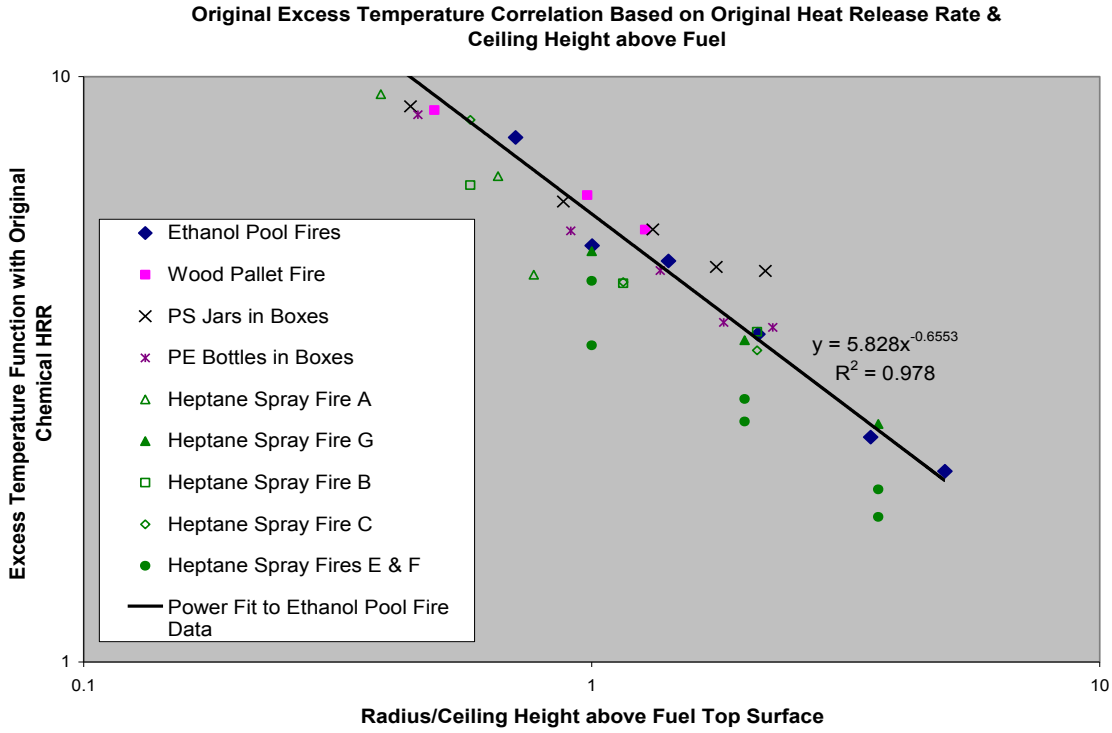

Figure 6 Re-analysis of Excess Temperature Data for Selected Fuels from the Original Ceiling Jet Temperature Correlation

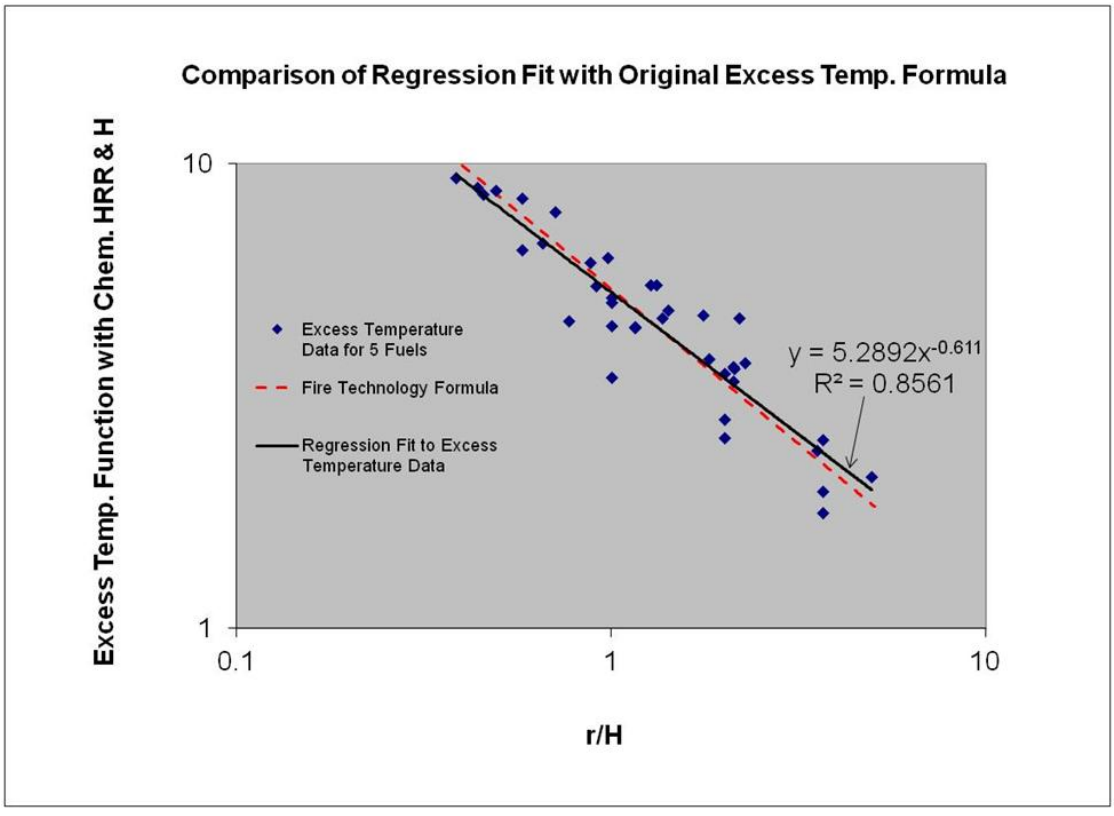

Figure 7 Comparison of Original Formula for Maximum Ceiling Jet Excess Temperature with Regression Fit (solid line) to Data from Figure 6

Here, the height, z_v, of the location for the virtual point source on the central axis of the fire is measured from the lowest elevation of continuous flaming, which for a pool fire is simply the pool surface and for a spray fire, the nozzle elevation. The ceiling height, z_H, would be measured from this same elevation. Note that the virtual height of the point fire source depends on the actual heat release rate and on the effective fuel diameter, D_{eff}. Thus, both a simple pool fire having a large surface area and the fire generated by the array of heptane sprays can be represented by a virtual point source.

With this new information about fire plume behavior, it should be possible to improve the ceiling jet velocity and temperature correlations by scaling velocity or excess temperature by the length, $z_H - z_v$, instead of H, the distance above the fuel top surface and by the convective heat release rate, $\dot{Q}_{conv}$ instead of heat release rate based on the chemical heat of combustion. For now, such a correlation improvement will be done using just ethanol pool and heptane spray fire data, not only because these are the best documented fire sources from the original study, in terms of combustion parameters, but because these are the only near steady-state fire sources. The fires in piles of solid fuels are inherently transient, which makes a data correlation difficult when transient velocity and temperature data are not available.

Handbook values[4] for heats of combustion for the two fuels selected are given in Table 3. Compared to what had been assumed in the previous study, the value of $\dot{Q}_{chem}$ is 13% greater for ethanol and 8% less for heptane. With these values for actual heats of combustion and for effective fuel diameters (Table 2 or Table ***4***) inserted in Equation 5, the virtual source heights shown in Table 4 can be obtained.

The new correlations for velocity and excess temperature with the virtual source correction are shown in *Figure 8* and***Figure*** *9*, respectively. The velocity function in the ordinate of *Figure* ***8*** is:

$$\frac{V_{\max}\left(z_H - z_v\right)^{1/3}}{\dot{Q}_{conv}^{\ 1/3}} \quad \frac{m^{4/3}}{s \times kW^{1/3}}$$

while the excess temperature function in the ordinate of *Figure* ***9*** is:

$$\frac{\left(T_{\max} - T_\infty\right)\left(z_H - z_v\right)^{5/3}}{\dot{Q}_{conv}^{\ 2/3}} \quad \frac{K \times m^{5/3}}{kW^{2/3}}$$

Fuel Type	***Chemical Heat of Combustion***[4] ***[kJ/g]***	***Convective Heat of Combustion***[4] ***[kJ/g]***
Ethanol Pool	25.60	19.00
Heptane Sprays	41.2	27.6

Table 3 Handbook Values for Chemical (Actual) and Convective Heats of Combustion for Ethanol and Heptane

Fuel Type	*Effective Diameter of Fuel [m]*	*Fuel Flow or Mass Loss Rate [g/s]*	*Chemical HRR [kW]*	*Virtual Origin Height above Base of Burning Fuel, [m]*	*Ceiling Height above Virtual Origin, [m]*	*Convective HRR [kW]*
Ethanol Pool	1.09	24.18	619.0	-0.0227	8.63	459.4
Heptane Spray A	3.66	173.6	7,153	-0.8409	8.77	4,792
Heptane Spray B	3.66	303.8	12,518	-0.1159	8.04	8,386
Heptane Spray C	3.66	434.1	17,883	0.4385	7.48	11,980
Heptane Spray D	3.66	520.9	21,460	0.7539	7.17	14,376
Heptane Spray E	3.66	173.6	7,153	-0.8409	5.41	4,792
Heptane Spray F	3.66	303.8	12,518	-0.1159	4.69	8,386
Heptane Spray G	3.66	434.1	17,883	0.4385	4.13	11,980

Table 4 Fire Source Conditions for the Ethanol Pool and Heptane Spray Fires Based on Handbook Values for Heats of Combustion

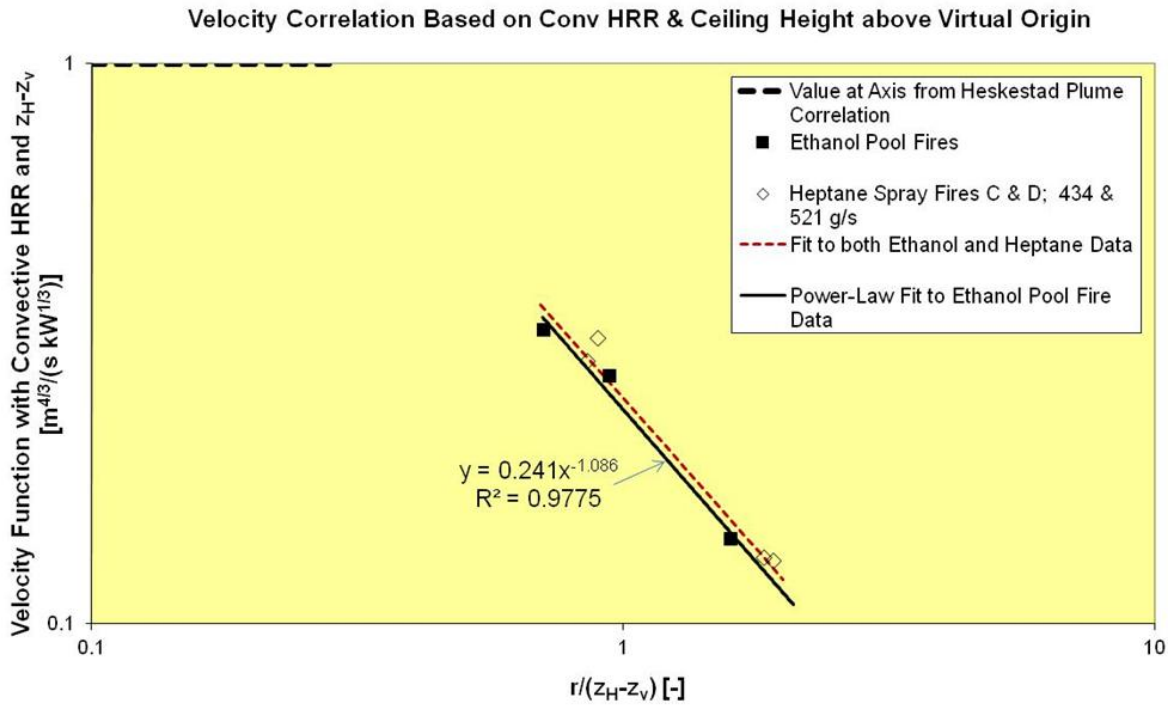

Figure 8 New Correlation for Ceiling Jet Velocity Based on Best Documented Fires Sources from the Original Study[1,2]

It can be seen by comparing *Figure 8* and***Figure 9*** with the previous *Figure 5* and*Figure 7* that the use of convective heat release rate and a virtual source improve the correlation of velocity and excess temperature data for the heptane sprays substantially. For both the heptane spray and ethanol pool data taken together, the resulting regression fit equations (dotted lines in *Figure 8* and***Figure 9***) and regression coefficients (R^2 values) are given below:

$$V_{\max} = 0.2526 \frac{\dot{Q}_c^{1/3}}{(z_H - z_v)^{1/3}} \left(\frac{r}{z_H - z_v} \right)^{-1.0739} \qquad R^2 = 0.972 \quad \text{for} \quad \frac{r}{z_H - z_v} > 0.246 \qquad (5)$$

$$T_{\max} - T_\infty = 6.721 \frac{\dot{Q}_c^{2/3}}{(z_H - z_v)^{5/3}} \left(\frac{r}{z_H - z_v} \right)^{-0.6545} \qquad R^2 = 0.958 \quad \text{for} \quad \frac{r}{z_H - z_v} > 0.134 \qquad (6)$$

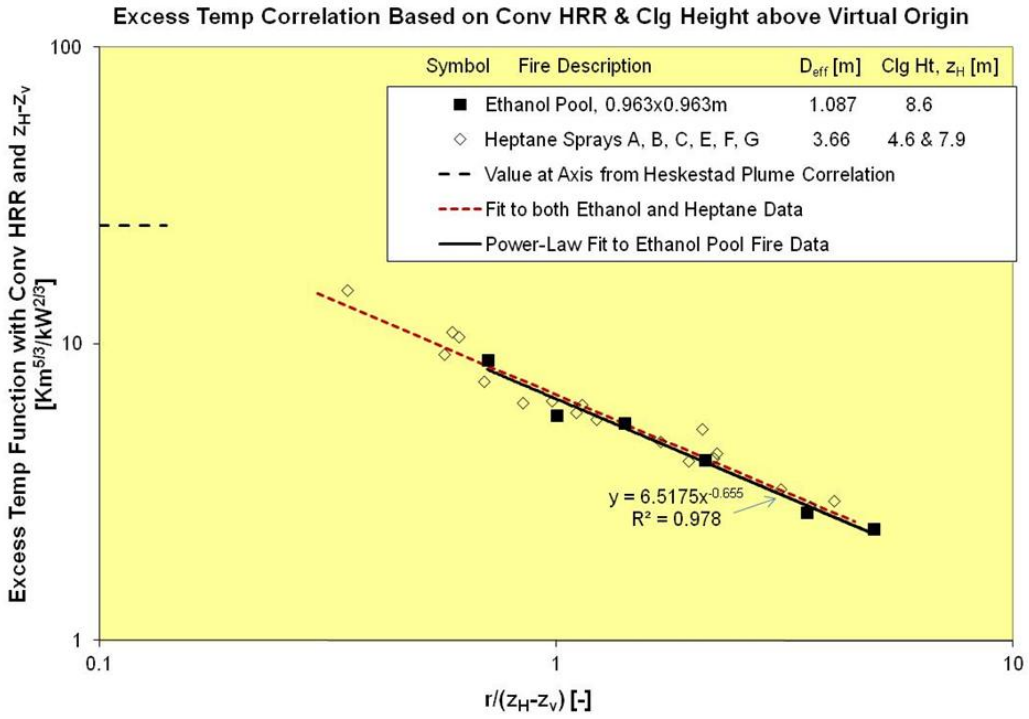

Figure 9 New Correlation for Ceiling Jet Excess Temperature Based on Best Documented Fire Sources from the Original Study[1,2]

In addition to the data correlations, *Figure 8* and***Figure 9*** show the respective velocity magnitude and excess temperature value at the plume axis, following Heskestad's formulas[5], as well as separate regression fits and coefficients for just the ethanol pool fires. By assuming that the maximum (i.e., at the plume axis) excess temperature and the magnitude of the maximum upward plume velocity remain invariant as the flow direction changes in the turning region (see Figure 1), a radial position can be found for which the ceiling jet correlations give the same result as the plume correlations (i.e., the plume and ceiling jet

correlations intersect). This determines the radial position limits in Equations 5 and 6 for which the ceiling jet correlation can begin to be applied.

These correlation equations for ceiling jet excess temperature and velocity, coupled with predictions from the integral model[1] and laboratory-scale measurements[6] of radial variations in ceiling jet thickness, enable the response of ceiling-mounted detectors and the activation of ceiling-mounted suppression devices to be predicted easily and quickly.

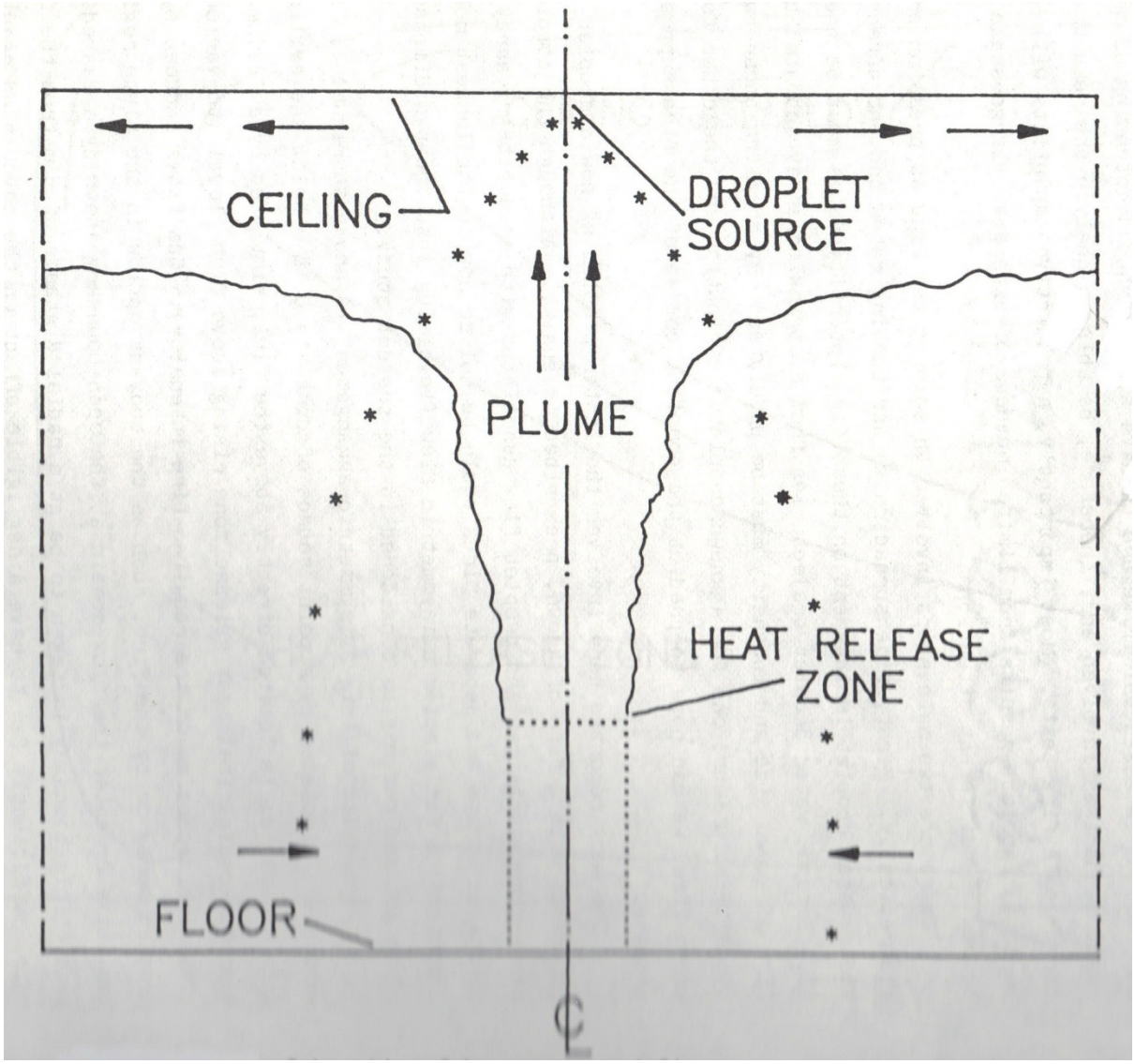

Figure 10 Schematic of the Interaction Resulting from a Fire Source Directly below a Droplet Spray

INTERACTIONS OF A PLUME & CEILING JET WITH A DROPLET SRAY

In order to determine if a droplet spray activated by the ceiling jet flow will be effective in suppressing a fire source, the interaction of the spray droplets with the fire induced flow must be understood and modeled. Such modeling would not only allow the amount of suppression agent reaching the seat of the fire to be predicted but also the final number of spray devices activated at the ceiling during fire growth and decay. The latter process, controlled partly by deflection of droplets by the fire-induced flow (impinging on and so delaying device

activation) and partly by cooling of the ceiling jet flow by activated sprays, is important for predicting the final flow of suppression agent demanded by the system. One of the first attempts to model these processes was in the mid-1980's when the idealized axisymmetric geometry of a spray source near a ceiling and directly above a fire source was examined[7]. Although this is an idealization to maintain symmetry and reduce computational time, it is also a practical problem because a large fire directly below a suppression device can prevent successful droplet penetration through the flames and onto the burning fuel. Shown in *Figure **10*** is a schematic of the flow interaction region that was being modeled, the gas motion through an iterative Eulerian solution using the TEACH CFD software and the droplets through a Lagrangian tracking solution for the order of 10 droplet sizes and initial trajectory angles[8].

In *Figure **10***, the dashed outer radius of the flow interaction region is a constant pressure boundary that allows for inflow and outflow, while the heat release zone contains a constant release of energy per unit volume to simulate a fire source. After several iterations of the gas flow calculation, droplets are injected at a velocity characteristic of the spray sprinkler and agent pressure being simulated. As a result of the droplet trajectory calculations for the range of drop sizes and injection angles being considered, mass, momentum and energy from the droplets are deposited into the Eulerian gas cells for succeeding iterations of the flow solution. Eventually, convergence to a steady-state solution is achieved.

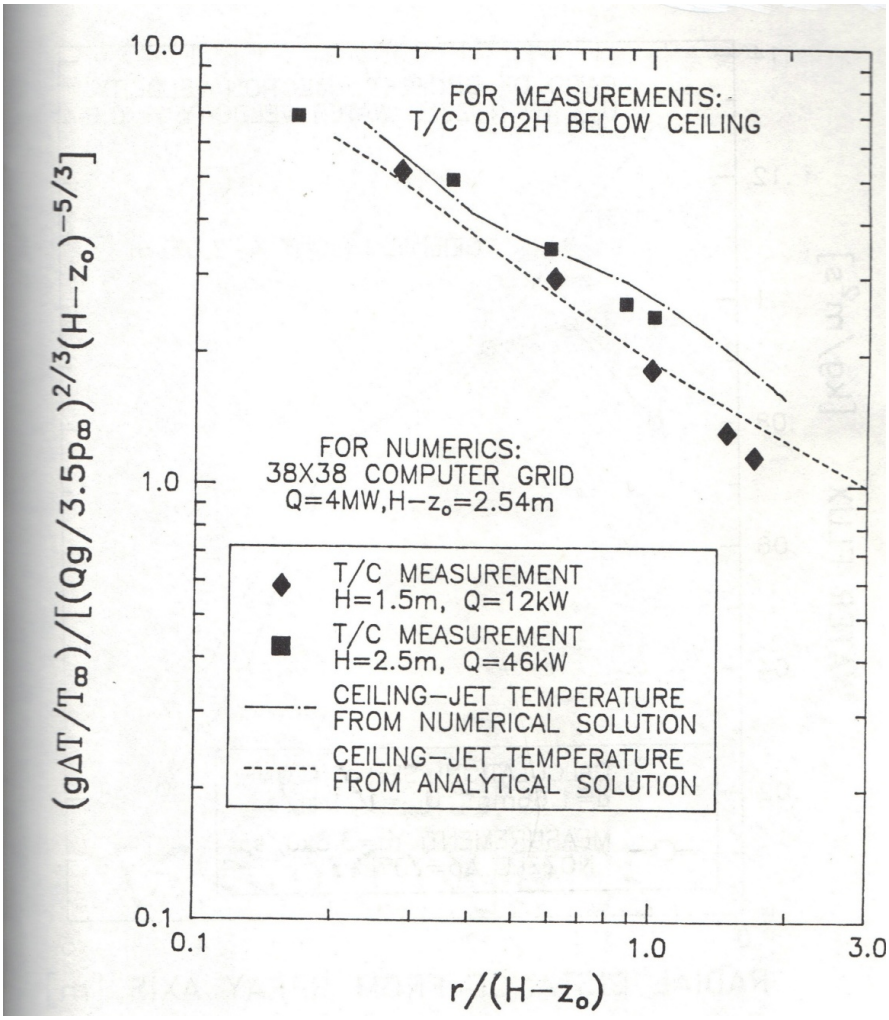

Figure 11 Comparison of CFD Calculations and Experimental Measurements of Excess Temperature in the Ceiling Jet

Partial confirmation of the validity of the flow interaction calculations was obtained through calculations first with a droplet spray alone and then with a fire source alone. For the calculations with a spray alone, an induced downward airflow to generate a floor jet and a distribution of droplet mass flux at floor level were observed that were comparable to observations made previously during sprinkler tests. For calculations with the fire source alone, a plume and ceiling jet flow was observed. A comparison of these calculation results with experimental data for one such case is shown in *Figure **11***, where excess temperatures measured in the ceiling jet appear to be in good agreement with the CFD calculations.

With some confidence that the calculation method was valid, the interaction of a plume flow with sprinkler droplets was investigated. One case where the plume associated with a fire heat release rate of 3.8 MW interacts with relatively small droplets (0.5 mm diameter) from a sprinkler spray directly above the heat release zone (dotted rectangle) is shown in *Figure 12*. Note that the heat release cylinder is nearly 2 m high in order to produce this high heat release rate at a volumetric rate of heat release typical of real flames. It can be seen from the streamline and droplet trajectory plot in this figure that the strong plume deflects the small droplets so that they reach the floor between 1.5 and 2 m from the fire axis, thereby preventing these droplets from reaching the base of the fire. The accumulation of droplets

near the 1.75 m location seems to generate an eddy within the plume entrained air flow near the floor. Corresponding isotherm plots would show how the ceiling flow is cooled by droplet evaporation.

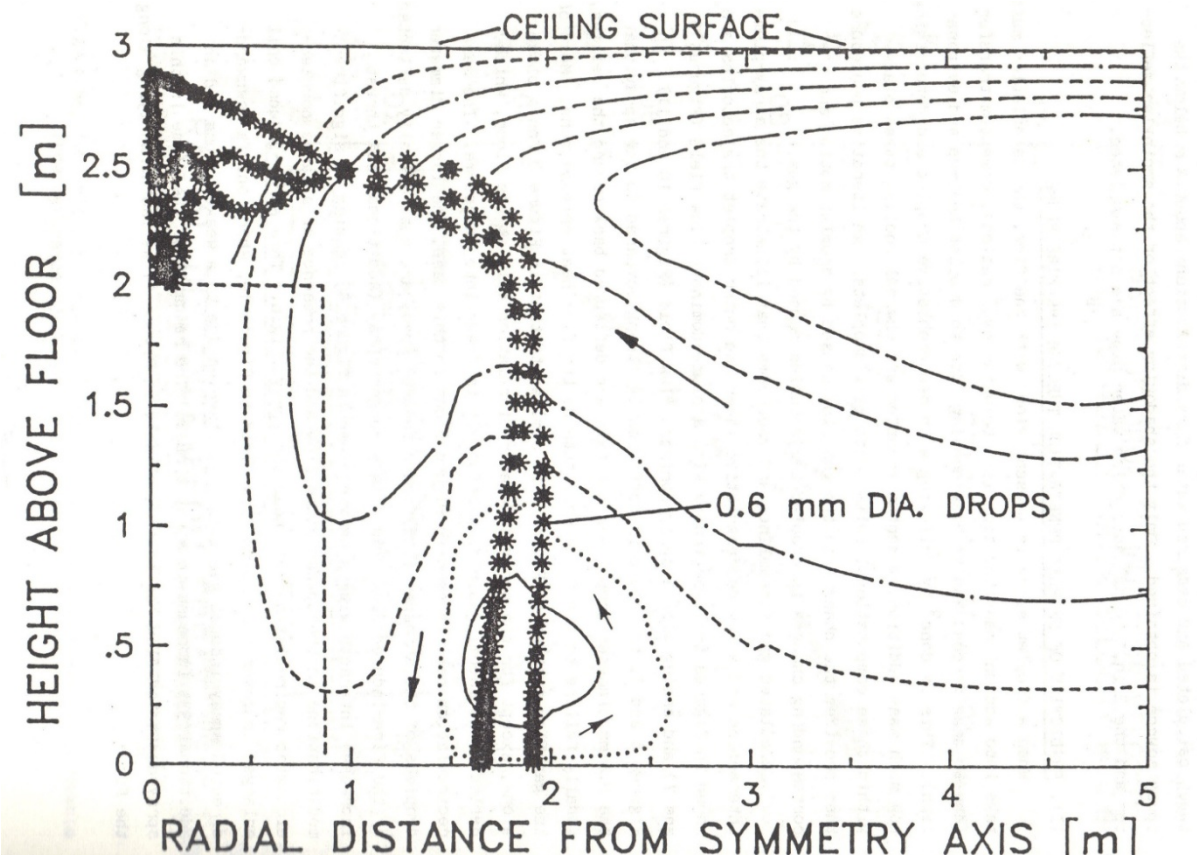

Figure 12 Gas streamlines (broken lines) and trajectories of 0.6 mm diameter droplets (asterisk symbols) resulting from the interaction of upward plume flow from a 3.8 MW simulated fire with the droplet spray from a point nozzle (water flow is 4.65 kg/s; droplet injection velocity is 8 m/s)

A second spray-plume interaction case is shown in *Figure 13*, where it can be seen that instead of the spray trajectories being strongly deflected by the plume flow (as in the previous figure), now a much weaker, 0.5 MW plume is evidently distorted by the larger momentum of the 1 mm diameter spray droplets. Note the much smaller heat release zone cylinder in *Figure 13* compared to that in *Figure 12*. The 1 mm droplet trajectories show virtually no effect from the plume flow but the plume flow is prevented by the droplet momentum from reaching the immediate vicinity of the spray nozzle. A large recirculation eddy near the ceiling seems to result from this particular interaction, as seen from the streamline plot in Figure 13.

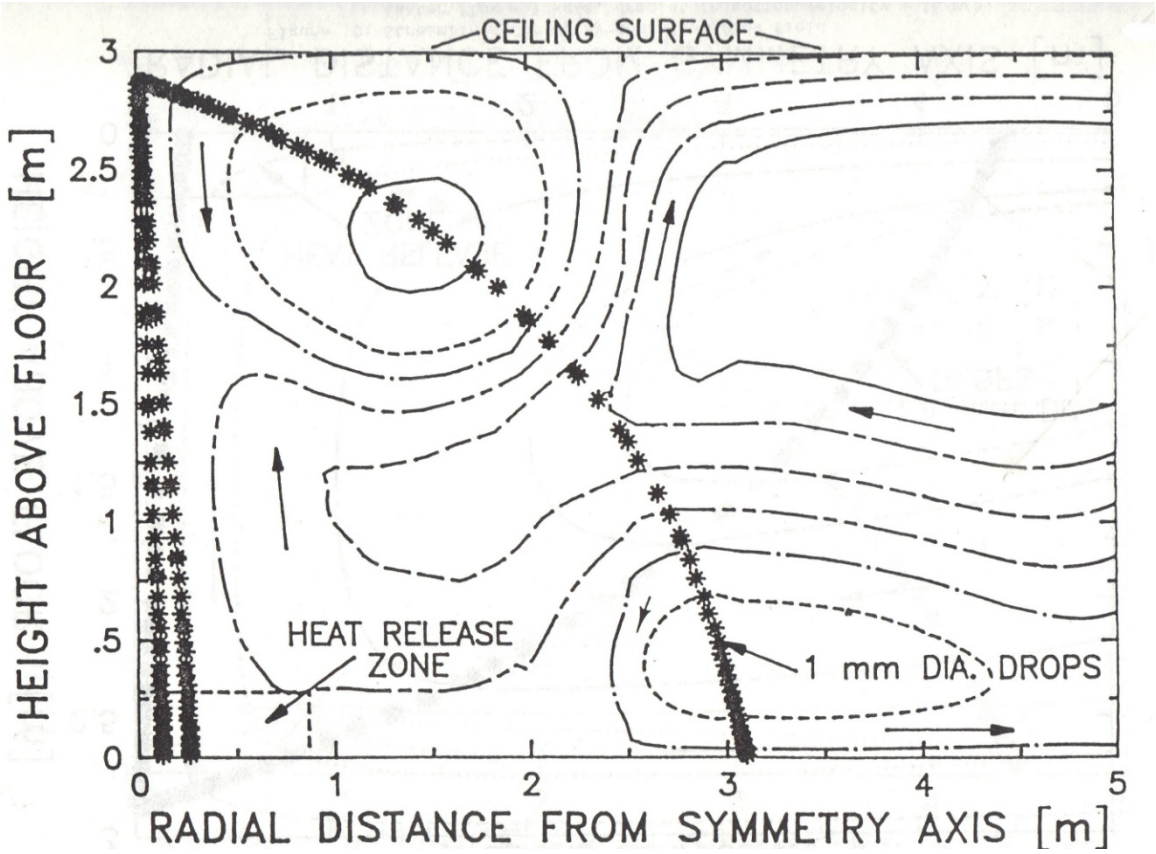

Figure 13 Gas streamlines (broken lines) and trajectories of 1 mm diameter droplets (asterisk symbols) resulting from the interaction of upward plume flow from a 0.5 MW simulated fire with the droplet spray from a point nozzle (water flow is 7 kg/s; droplet injection velocity is 12 m/s)

Because it is important to determine the amount of suppression agent reaching the "seat" of the fire (the base of the heat release cylinder in this case), numbers of CFD calculations similar to those in *Figure 12* and *Figure **13*** were run to reproduce conditions both with a simulated fire and without the fire present, the latter to calculate the "undisturbed" or "baseline" droplet mass flux. Generally, the amount of agent reaching the base of the heat release cylinder is measurably less when a fire is being simulated than when the heat release rate is zero, the ratio of the former with the latter termed the penetration ratio.

Figure 14 shows how this ratio varies for a fixed ceiling (i.e., nozzle height) and fire configuration but changing droplet spray properties. Note that each data point in the figure represents two sets of calculations, one with a simulated fire and one without. As expected, the maximum amount of available suppression agent arrives at the base of the heat release region when the vertical component of the spray momentum flow rate is much greater than that in the plume (both at the spray nozzle location) and the spray droplet size is much greater than the critical drop size (for overcoming the plume up-flow when released with zero velocity at the nozzle location). Note that both the plume momentum flow and the critical drop size are calculated a priori from correlation formulas once the nozzle height and the fire heat release are specified. Conversely, when the function of momentum and droplet size is less than about 0.5 for this 4 MW fire, very little suppression agent can reach the base of the heat release zone.

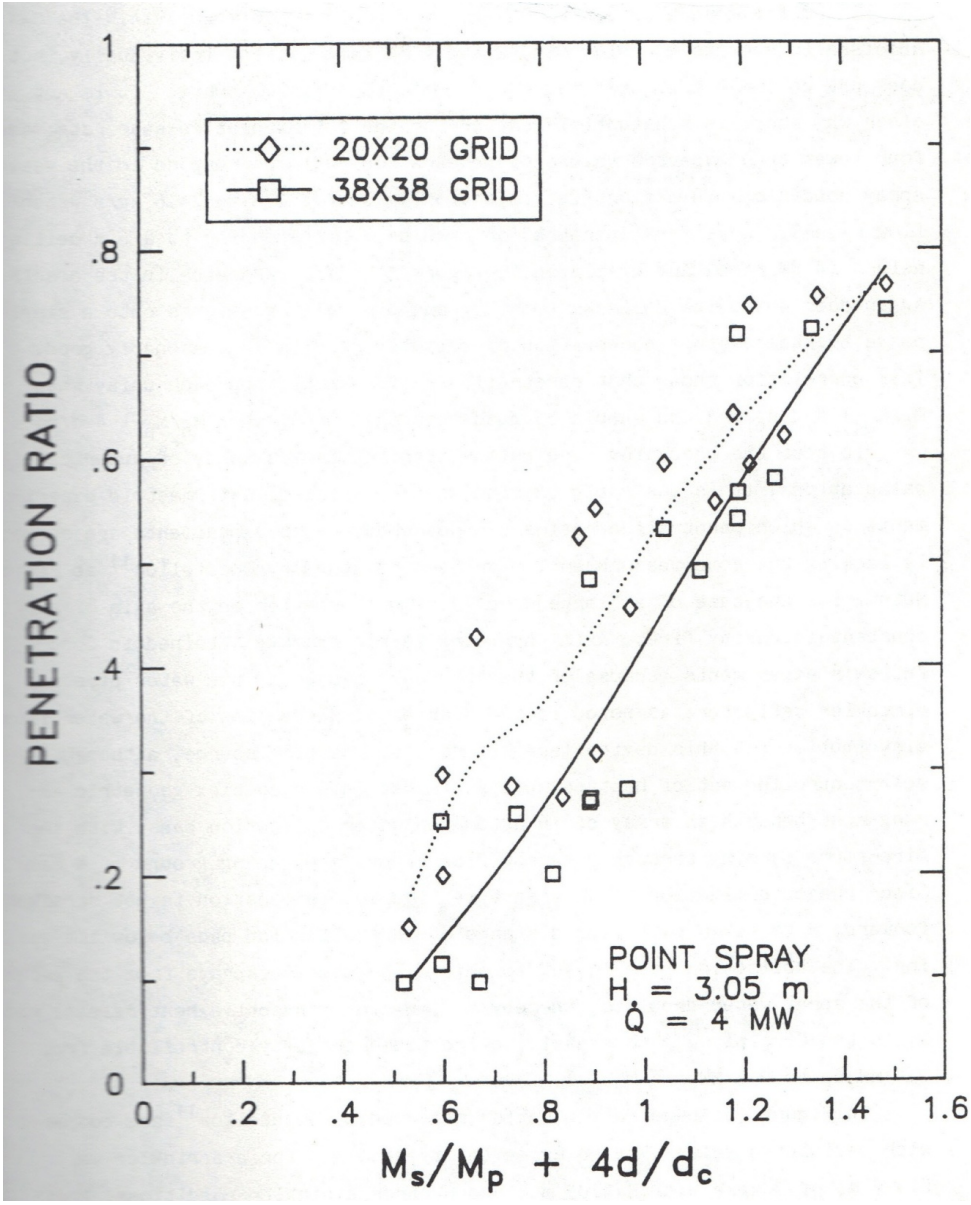

Figure 14 Ratio of water flow reaching near the base of the heat release zone in the presence of a simulated 4 MW fire to that when there is no fire (Penetration Ratio) as a function of both the ratio of spray vertical momentum flow to plume vertical momentum flow, M_s/M_p and the ratio of mass-median droplet diameter to critical droplet diameter, d/d_c at the spray nozzle location.

In addition to the success of droplet agent in penetrating the fire plume and cooling the ceiling jet, the numerical method was also used to calculate the flux of plume-deflected droplets within the ceiling flow at a typical location of another sprinkler nozzle. This type of calculation showed that there was a narrow range of the function of momentum and droplet size ratios for which this flux is greater than a critical impingement rate. The critical rate of impingement of agent droplets on a sprinkler heat sensing element is the flux needed to continuously absorb all fire-induced heat transfer while maintaining an element temperature below the detection level.

Some attempts were made to confirm the CFD interaction calculations, especially those for spray penetration, using data from sprinklered fire experiments but with varying degrees of

success. The experimental measurement of spray penetration during a fire is itself very difficult and had not been thoroughly perfected at the time the calculations were done.

MINIMUM AGENT FLUX FOR FIRE SUPPRESSION

The preceding discussion has shown that it is possible to predict when suppression agent will begin to flow from nozzles in the ceiling jet induced by a fire and how much of that agent flow will reach potential locations of burning fuel. Now, it must be determined just how much agent is necessary to prevent fire growth, i.e., to suppress the fire, even if complete extinguishment is not achieved. One method to achieve that goal is to determine the flame heat flux within the fuel array where fire growth is a concern and then insure that sufficient agent flux from ceiling sprays arrives within the fuel array to absorb that heat flux. In this way, fire suppression can be achieved.

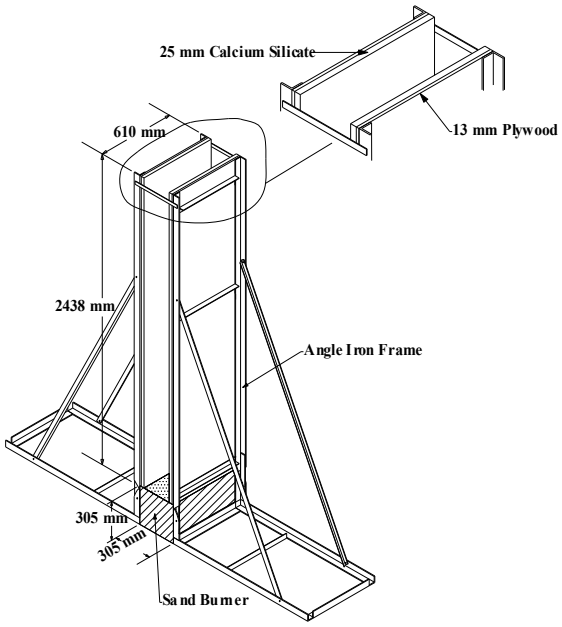

Figure 15 Fire Test of a Combustible Material in a Parallel Surface Arrangement[9]

Most fuel arrays that are dangerous, such as high piled storage or rack storage of polymer items in boxes, have flue spaces where flames can propagate rapidly and lead to a growing fire heat release rate. The essential element of such a flue space can be represented by the geometric arrangement in *Figure 15*, where two facing panels of the material to be tested are mounted atop a sand burner. With this arrangement[9], radiant heat from the sand burner flame (typically a 60-100kW propane flame) and from the flame of the test material itself is effectively trapped due to the 2:1 ratio of panel width to separation distance, effectively reproducing the environment of many full-scale fire scenarios. At the same time, there is ample access for air to insure that all flames are well ventilated and easy access for instruments to measure flame heat flux between the panels.

If fire growth on the test material occurs in this simplified flue space, it is self evident because the height of the burner flame is typically only of the order of the width of the panels. Note that the total heat release rate in this arrangement can easily be measured by

using a combustion products collector suspended above the apparatus. Note also that the simplified geometry increases the likelihood for success of a predictive model of the fire growth process.

To determine the peak flame heat flux that must be absorbed by agent droplets (e.g., through evaporation of a film or layer on the burning fuel) for fire suppression, it will be necessary to measure heat flux at several locations within the prototype flue represented in *Figure 15*. To do this, fairly rugged heat flux gauges would ordinarily be necessary. An alternative[10] is the use of the "heat flux pipe" shown in *Figure 16*. This rugged instrument consists of a pipe (see item #1 in the figure) in which a turbulent water flow is forced through a spiral channel adjacent to the inside surface of the pipe. A set of thermocouples (one every 16% of pipe length) records changes in water temperature as the flow very rapidly responds to heat flux from flames adjacent to the pipe. As a result, a fairly accurate flame heat flux profile is obtained. The instrument could be used not only in the prototype flue but within the flues of actual storage arrays. With this information, the minimum flux of agent droplets to the surface of the flue that will cause fire suppression through heat flux absorption can be determined.

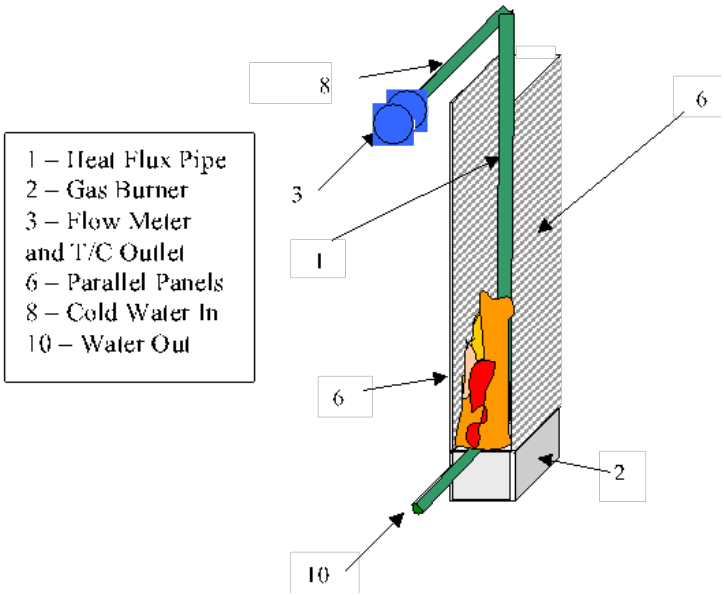

Figure 16 Schematic of How a Heat Flux Pipe Is Used in a Prototype Flue[10]

CONCLUSIONS

A reexamination of data underlying the 1972 ceiling jet formulas[2] has produced new regression fits that should be more reliable than the original formulas since only data from steady, well-documented fire sources are included. Such algebraic formulas are useful for predicting detection/activation times of ceiling mounted devices, e.g., fire sprinklers. To determine what mass flux of agent droplets from these activated sprinklers arrives at the fire source, it is shown that CFD coupled with droplet trajectory calculations[7] have been used beginning in the mid-1980's to quantify the interaction between the fire induced plume/ceiling jet flow and droplet sprays. Finally, one method is described for obtaining the

minimum flux of agent droplets arriving at a burning fuel surface that is required to successfully suppress a fire.

REFERENCES

1 Alpert, R.L. (1975) "*Turbulent Ceiling Jet Induced by Large-Scale Fires*" Combustion Science and Technology, Volume 11, p. 197.

2 Alpert, R.L. (1972) "*Calculation of Response Time of Ceiling-Mounted Fire Detectors*" Fire Technology, Volume 8, p. 181.

3 Alpert, R.L. (1971) "*Fire Induced Turbulent Ceiling-Jet*" Factory Mutual Research Corporation, Norwood, MA USA, Technical Report Serial No. 19722-2

4 Tewarson, A. (2008) "*Generation of Heat and Gaseous, Liquid and Solid Products in a Fire*" in "*The SFPE Handbook of Fire Protection Engineering*" (4th Edition) National Fire Protection Association, Quincy, MA USA, pp. 3-109 to 3-194, ISBN-13: 978-0-87765-821-4.

5 Heskestad, G., "*Fire Plumes, Flame Height and Air Entrainment*" in "*The SFPE Handbook of Fire Protection Engineering*" (4th Edition) National Fire Protection Association, Quincy, MA USA, pp. 2-1 to 2-20, ISBN-13: 978-0-87765-821-4.

6 Motevalli, V. and Marks, C.H., "*Characterizing the Unconfined Ceiling Jet under Steady-State Conditions: A Reassessment*" in "*Fire Safety Science, Proceedings of the Third International Symposium*" (1991) Elsevier Applied Science, New York, p. 301.

7 Alpert, R.L., "*Numerical Modeling of the Interaction between Automatic Sprinkler Sprays and Fire Plumes*" (1985) Fire Safety Journal, Volume 9, pp. 157-163.

8 Crowe, C.T., Sharma, M.P. and Stock, D.E. (1977) "*The Paricle-Source-in-Cell Model for Gas Droplet Flows*" Journal of Fluids Engineering, Volume 99, p. 325.

9 Alpert, R.L. (2003) "*Evaluation of the Hazard of Fire Resistant Materials Using Measurements from Laboratory and Parallel Panel Tests*" in "*Fire Safety Science-Proceedings of the Seventh International Symposium*" International Association for Fire Safety Science, London, ISBN 0-9545348-0-8, pp. 41-57.

10 Wu, P., Orloff, L., Chaffee, J., de Ris, J. and Alpert, R.L. (2004) "*Flame Heat Transfer in Commodity Classification Fire Tests*" in "*10th International Fire Science and Engineering Conference Proceedings*", Interflam2004, Interscience Communications, London.